Sensors and Materials, Vol. 34, No. 12 (2022) 4491–4505
MYU Tokyo

S & M 3124

Recovery of Abnormal Data for Bridge Structural Health Monitoring Based on Deep Learning and Temporal Correlation

Hanwen Ju,[1] Yang Deng,[1,2*] Wenqiang Zhai,[1] and Aiqun Li[1,2]

[1]School of Civil and Transportation Engineering,
Beijing University of Civil Engineering and Architecture, Beijing 100044, China
[2]Beijing Key Laboratory of Functional Materials for Building Structure and Environment Remediation,
Beijing University of Civil Engineering and Architecture, Beijing 100044, China

(Received June 27, 2022; accepted October 13, 2022)

Keywords: structural health monitoring, abnormal data recovery, deep learning, neural network, temporal correlation

Structural health monitoring is of great significance to prevent structural disasters. However, the sensors in the structure monitoring system inevitably produce a large number of abnormal data. To ensure the integrity and practicability of monitoring data, it is necessary to recover abnormal monitoring data. Most existing data recovery methods use the correlation between variables and spatial correlation, rather than fully mine the temporal correlation of data. An abnormal data recovery framework based on a gated recurrent unit (GRU) neural network and temporal correlation is proposed in this study. The abnormal data recovery framework can be independent of other sensors. The input and output configurations of the GRU model are optimized. Bidirectional prediction including forward and backward prediction information is used to improve the prediction accuracy of the model. The framework is demonstrated using monitoring data of beam-end displacement and pylon tower tilt collected from Waitan Bridge in Ningbo, China. The results show that the framework has high accuracy in abnormal data recovery. After data recovery, the linear relationship between structural response and temperature is significantly improved.

1. Introduction

Structural health monitoring systems are widely used in civil engineering.[1,2] However, due to power failure, network failure, electromagnetic interference, and other factors, sensors inevitably produce a large number of abnormal monitoring data.[3,4] These abnormal monitoring data may interfere with the structural state analysis and cause false and missing reports of structural problems.[5] The elimination of more abnormal monitoring data will cause serious data loss, adversely affecting the practical application of structural monitoring data.[6,7] To ensure the integrity and practicability of structural monitoring data, it is necessary to recover abnormal monitoring data.

*Corresponding author: e-mail: dengyang@bucea.edu.cn
https://doi.org/10.18494/SAM4000

ISSN 0914-4935

For a long time, data nearest neighbor (NN) imputation methods have been widely used in the recovery of structural monitoring data.[8] However, simple data imputation cannot easily recover long sequences of missing data. To fully mine the correlation between data, statistical and machine learning methods are also used to recover structural abnormal monitoring data. On the one hand, some studies have focused on the correlation between different variables and have recovered abnormal data through the correlation model between different variables.[9,10] Wan and Ni proposed a Bayesian multitask learning method based on the covariance function to recover the abnormal data, and they recovered the acceleration data through the correlation between acceleration and temperature monitoring data.[10] On the other hand, the spatial correlation of structural monitoring data has also been fully mined. Through the spatial correlation of sensors, abnormal monitoring data can also be recovered.[11–13] Ma *et al.* used Gaussian process regression (GPR) technology to reconstruct the dynamic nonlinear response of structures by simultaneously interpreting the spatial correlation of different sensors. This method was applied to restoring acceleration monitoring data of Canton Tower.[13]

With the development of computer and AI technology, a deep learning artificial neural network (ANN) has also been applied to the recovery of structural abnormal monitoring data. A deep learning neural network has major advantages in the nonlinear mapping of data and is suitable for data sequence prediction and recovery. Fan *et al.* proposed a method for recovering vibration monitoring data that was based on a convolution neural network (CNN), and they constructed the nonlinear relationship between incomplete vibration data and complete vibration data.[14] A recurrent neural network (RNN) has also been widely used in data sequence recovery and prediction.[15] Yuan *et al.* established a prediction model for dam deformation by using variational modal decomposition (VMD) and a long short-term memory (LSTM) neural network.[16]

In general, the existing studies on the recovery of structural abnormal monitoring data based on a deep learning neural network can be summarized as follows. (i) The existing studies on abnormal data recovery mainly focus on mining the variable correlation and spatial correlation, but less on the mining time correlation. A cluster mode exists in the sensor fault of a structural health monitoring system.[5] When most sensors are disturbed, the variable correlation and spatial correlation of monitoring data may be difficult to use. (ii) Most studies use the neural network model of unidirectional training to predict the data sequence. The information after the abnormal data sequence is not fully used.

To solve the above problems, in this study we propose an abnormal data recovery framework based on a gated recurrent unit (GRU) neural network and temporal correlation. Firstly, we introduce the specific process of the abnormal data recovery framework. This framework reconstructs the input and output configurations of a neural network and uses bidirectional prediction to improve the prediction accuracy of the model. Secondly, the accuracy and effectiveness of the framework are verified by taking the beam-end displacement data and pylon tower tilt data in the structural monitoring system of Waitan Bridge in Ningbo, China. Finally, the abnormal data of beam-end displacement and pylon tower tilt are recovered by using the framework.

2. Abnormal Data Recovery Framework

2.1 Deep learning neural networks

A deep learning neural network has major advantages in the nonlinear mapping of data and is suitable for data sequence prediction and recovery.[17] Hence, in this study we adopt a GRU neural network for the abnormal data recovery framework. For comparison, we also use an LSTM neural network to recover abnormal monitoring data. The LSTM neural network can use not only current characteristic information, but also intermediate results generated by previous training.[18] The LSTM neural network and unit are shown in Fig. 1(a). The key formulas of the LSTM neural unit are as

$$\boldsymbol{f}_t = \sigma\left(\boldsymbol{W}_f \cdot \left[\boldsymbol{h}_{t-1}, \boldsymbol{x}_t\right]\right), \tag{1}$$

$$\boldsymbol{i}_t = \sigma\left(\boldsymbol{W}_i \cdot \left[\boldsymbol{h}_{t-1}, \boldsymbol{x}_t\right]\right), \tag{2}$$

$$\tilde{\boldsymbol{C}}_t = \tanh\left(\boldsymbol{W}_c \cdot \left[\boldsymbol{h}_{t-1}, \boldsymbol{x}_t\right]\right), \tag{3}$$

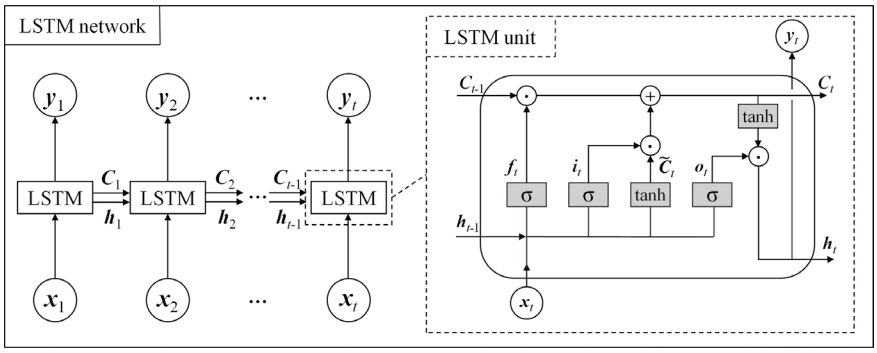

(a)

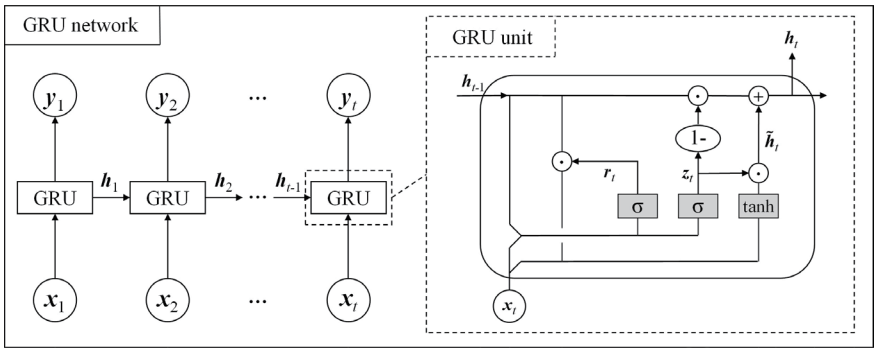

(b)

Fig. 1. Neural network structures: (a) LSTM and (b) GRU.

$$\boldsymbol{o}_t = \sigma\left(\boldsymbol{W}_o \cdot \left[\boldsymbol{h}_{t-1}, \boldsymbol{x}_t\right]\right), \tag{4}$$

$$\boldsymbol{C}_t = \boldsymbol{f}_t \cdot \boldsymbol{C}_{t-1} + \boldsymbol{i}_t \cdot \boldsymbol{C}_t, \tag{5}$$

$$\boldsymbol{y}_t = \boldsymbol{o}_t \cdot \tanh\left(\boldsymbol{C}_t\right), \tag{6}$$

where $\boldsymbol{C}_{t-1}$ and $\boldsymbol{C}_t$ are the unit states of the previous time and the current time; $\boldsymbol{h}_{t-1}$ is the unit output of the previous time; $\tilde{\boldsymbol{C}}_t$ is the candidate unit state at time t; $\boldsymbol{f}_t$, $\boldsymbol{i}_t$, and $\boldsymbol{o}_t$ are the statuses of the forget gate, input gate, and output gate at time t; $\boldsymbol{W}_f$, $\boldsymbol{W}_i$, $\boldsymbol{W}_c$, and $\boldsymbol{W}_o$ are the weight matrices of the forget gate, input gate, unit state, and output gate; $\boldsymbol{x}_t$ is the input of the network model at time t; $\boldsymbol{y}_t$ is the output of the network model at time t; σ(·) is a nonlinear activation function, where the sigmoid function is generally selected; and tanh(·) is the hyperbolic tangent function, respectively.

The GRU neural network and unit are shown in Fig. 1(b). The GRU neural network inherits the ability to deal with gradient problems from the LSTM neural network. Its gate structure can effectively filter out useless information and capture long-term dependences in time series data. The GRU neural network saves and updates useful information by controlling the opening and closing of the gates, offsetting the gradient in the process.[19] The key formulas of the GRU neural unit are

$$\boldsymbol{r}_t = \sigma\left(\boldsymbol{W}_o \cdot \left[\boldsymbol{h}_{t-1}, \boldsymbol{x}_t\right]\right), \tag{7}$$

$$z_t = \sigma\left(\boldsymbol{W}_z \cdot \left[\boldsymbol{h}_{t-1}, \boldsymbol{x}_t\right]\right), \tag{8}$$

$$\boldsymbol{h}_t = \tanh\left(\boldsymbol{W}_h \cdot \left[\boldsymbol{r}_t \cdot \boldsymbol{h}_{t-1}, \boldsymbol{x}_t\right]\right), \tag{9}$$

$$\boldsymbol{h}_t = \left(1 - z_t\right) \cdot \boldsymbol{h}_{t-1} + z_t \cdot \tilde{\boldsymbol{h}}_t, \tag{10}$$

$$\boldsymbol{y}_t = \sigma\left(\boldsymbol{W}_o \cdot \boldsymbol{h}_t\right), \tag{11}$$

where z_t is the reset gate state at time t; $\boldsymbol{r}_t$ is the update gate state at time t; $\tilde{\boldsymbol{h}}_t$ is the candidate unit state at time t; $\boldsymbol{h}_{t-1}$ and $\boldsymbol{h}_t$ are the unit states of the previous time and current time; $\boldsymbol{W}_r$, $\boldsymbol{W}_z$, $\boldsymbol{W}_{\tilde{h}}$, and $\boldsymbol{W}_o$ are weight matrices of the update gate, reset gate, candidate unit state, and output layer; σ(·) is a nonlinear activation function, where the sigmoid function is generally selected; $\boldsymbol{x}_t$ is the input of the network model at time t; $\boldsymbol{y}_t$ is the output of the network model at time t; and the tanh(·) function is the hyperbolic tangent function, respectively.

2.2 GRU-based data recovery framework

Most studies use environmental variable data (such as temperature and wind) and spatial correlation to recover structural monitoring data.[14–16] The neural network model usually takes environmental variable data or the adjacent sensor data as the input to recover the abnormal data.[5] The results of existing studies show that the recovery of abnormal data using the data correlation between adjacent sensors has high accuracy. However, environmental interference causes a large number of sensors to produce abnormal data. A cluster mode exists in the sensor fault of structural health monitoring systems. In a period of time, adjacent sensors may produce abnormal data such as drift, missing data, and outliers at the same time. The cluster mode makes it difficult to use spatial correlation. Hence, in this study, we propose an abnormal data recovery framework based on temporal correlation, which can be independent of other sensors. The framework uses the structural monitoring data of a period of time before the abnormal data as the input of the neural network model to predict the abnormal data sequence. The output data of the model at this time is used as the input of the model at the next time through a sliding window, and then the abnormal data of the whole sequence can be predicted and recovered. However, the simple forward-prediction model does not make full use of the information before and after abnormal data. The prediction accuracy of the neural network model for long-distance sequences usually decreases with increasing sequence length. Hence, in this study we propose a bidirectional prediction method. Bidirectional prediction can make full use of the information before and after abnormal data to improve the prediction accuracy of the model for long sequences. The recovery framework of abnormal data based on the GRU model and temporal correlation is shown in Fig. 2. The abnormal data recovery procedures are described below.

(i) The structural monitoring data are divided in accordance with the length of the abnormal data sequence. The structural monitoring sequences $\boldsymbol{X}^f = \left[X_1^f, X_2^f, \ldots, X_i^f, \ldots X_n^f \right]$ and $\boldsymbol{X}^b = \left[X_1^b, X_2^b, \ldots, X_i^b, \ldots, X_n^b \right]$ before and after the abnormal data sequence, respectively, are extracted. To avoid gradient vanishing and gradient explosion, each data sequence should be normalized.[20] Each data sequence is divided into a training set and test set. The training set is used as the training data of the model, and the test set is used to verify the accuracy and generalization ability of the model.

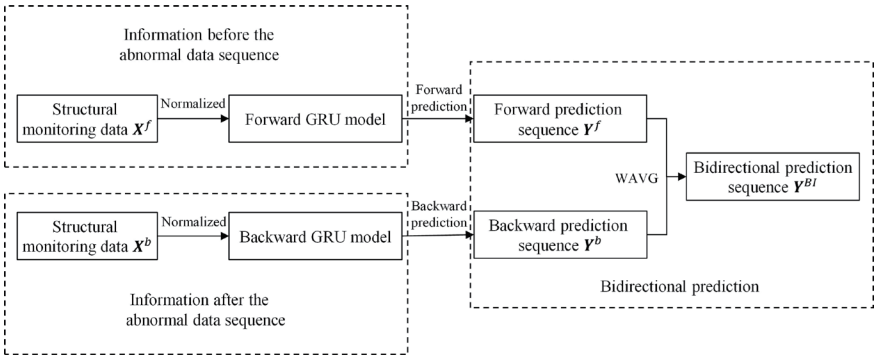

Fig. 2. Recovery framework of abnormal monitoring data.

(ii) The GRU neural network model, which consists of an input layer, GRU layer, fully connected layer, and output layer, is constructed and trained. The input sequence of forward model training is $\boldsymbol{X}^{f}_{output}$, $\boldsymbol{X}^{f}_{output,i}$ =[X^{f}_{i-2}, X^{f}_{i-1}]^{T}, and the output sequence is $\boldsymbol{X}^{f}_{output}$, $\boldsymbol{X}^{f}_{output,i}$ = [X^{f}_{i}]. The input sequence of backward model training is $\boldsymbol{X}^{b}_{input}$, $\boldsymbol{X}^{b}_{input,i}$ =[X^{b}_{i+2}, X^{b}_{i+1}]^{T}, and the output sequence is $\boldsymbol{X}^{f}_{output}$, $\boldsymbol{X}^{f}_{output,i}$ = [X^{b}_{i}].

(iii) The trained neural network model is used for bidirectional prediction of the abnormal data sequence. The forward GRU model is used to predict the abnormal data sequence, and the forward-prediction sequence $\boldsymbol{Y}^{f}=\left[Y^{f}_{1},Y^{f}_{2},\ldots,Y^{f}_{i},\ldots Y^{f}_{n}\right]$ is obtained. The backward GRU model is also used to predict the abnormal data sequence, and the backward prediction sequence $\boldsymbol{Y}^{b}=\left[Y^{b}_{1},Y^{b}_{2},\ldots,Y^{b}_{i},\ldots,Y^{b}_{n}\right]$ is obtained. The bidirectional prediction sequence $\boldsymbol{Y}^{BI}=\left[Y^{BI}_{1},Y^{BI}_{2},\ldots,Y^{BI}_{i},\ldots,Y^{BI}_{n}\right]$ is calculated using Eq. (12). The bidirectional prediction sequence is used to recover abnormal data.

$$\boldsymbol{Y}^{BI}_{i}=\begin{cases}\dfrac{Y^{f}_{i}+Y^{b}_{i}}{2} & (n=1)\\ \dfrac{n-i}{n-1}Y^{f}_{i}+\dfrac{i-1}{n-1}Y^{b}_{i} & (n>1)\end{cases} \tag{12}$$

3. Case Study: Cable-stayed Bridge

3.1 Monitoring system

The structural monitoring data of Waitan Bridge in Ningbo city, Zhejiang province, China are used to verify the accuracy of the proposed data recovery framework. As shown in Fig. 3, Waitan Bridge is an irregularly shaped cable-stayed bridge. The main beam adopts a separated steel box girder and is connected as a whole through a cross beam. The main tower adopts a triangular inclined tower structure composed of four parts: the front pylon, the upper tower head anchorage zone, the rear inclined rod, and the horizontal rod. The main tower is located in the middle of two separated girders. The structure monitoring system includes six pylon tower tilt sensors, four beam-end displacement sensors, and three structure temperature sensors. Four beam-end displacement sensors each are installed at the beam ends of the upstream and downstream main beams. Four pylon tower tilt sensors are installed at the front pylon and two are installed at the rear inclined rod. Two structural temperature sensors are installed at the main beam and one is installed in the anchorage zone of the upper tower head. Figure 3 shows the location of each sensor. The monitoring data are collected every 2 min.

3.2 Configuration of input and output

Taking the monitoring data of beam-end displacement sensor BDS_1-1 and pylon tower tilt sensor PTS_1-1 from May 1 to May 9, 2020 as an example, the optimization process of the GRU neural network model is demonstrated. As shown in Fig. 4, each sequence contains 6480 data points. The data segment containing 2160 data points in the middle of the data sequence is

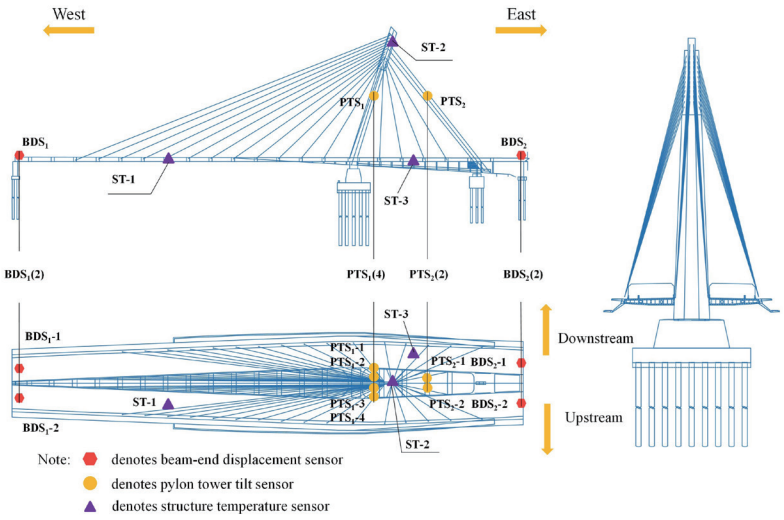

Fig. 3. (Color online) Structure monitoring system of Waitan Bridge.

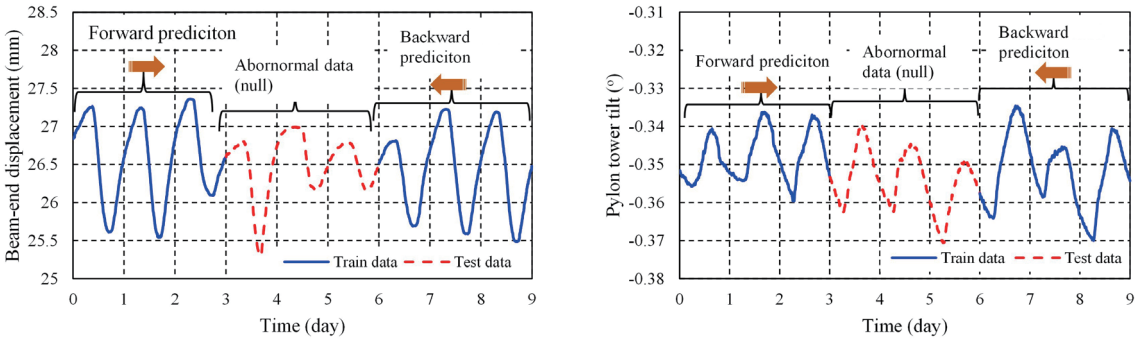

Fig. 4. (Color online) Monitoring data sequences: (a) beam-end displacement and (b) pylon tower tilt.

selected as the test data sequence, and the 2160 data points before and after the test data sequence are used as the training data for forward and backward prediction, respectively.

GRU and LSTM neural networks have strong ability to deal with the nonlinear mapping of time series. In this study, these two neural networks are used to recover the test data in Fig. 4 by using the prediction capacity of neural networks, and the prediction accuracy of the two neural networks is compared. Compared with the hyperparameters of the neural network, the configuration of the neural network input layer has a greater impact on the prediction results.[21] Hence, it is necessary to investigate the prediction accuracy of the neural network with different input configurations. Taking the beam-end displacement and pylon tower tilt data as an example, the input layers of the GRU and LSTM neural networks are reconstructed. The left training data

sequence in Fig. 4 is used to train the neural network, and the middle test data sequence is used to test the accuracy of the forward-prediction neural network model. The input $\boldsymbol{X}_{input}^{f}$ and output $\boldsymbol{X}_{output}^{f}$ are constructed using the following equations.

Model-I

$$\begin{aligned} \boldsymbol{X}_{input}^{f} &= \begin{bmatrix} X_1 & X_2 & \cdots & X_{n-1} \end{bmatrix} \\ \boldsymbol{X}_{output}^{f} &= \begin{bmatrix} X_2 & X_3 & \cdots & X_n \end{bmatrix} \end{aligned} \tag{13}$$

Model-II

$$\begin{aligned} \boldsymbol{X}_{input}^{f} &= \begin{bmatrix} X_1 & X_2 & \cdots & X_{n-2} \\ X_2 & X_3 & \cdots & X_{n-1} \end{bmatrix} \\ \boldsymbol{X}_{output}^{f} &= \begin{bmatrix} X_3 & X_4 & \cdots & X_n \end{bmatrix} \end{aligned} \tag{14}$$

Model-III

$$\begin{aligned} \boldsymbol{X}_{input}^{f} &= \begin{bmatrix} X_1 & X_2 & \cdots & X_{n-3} \\ X_2 & X_3 & \cdots & X_{n-2} \\ X_3 & X_4 & \cdots & X_{n-1} \end{bmatrix} \\ \boldsymbol{X}_{output}^{f} &= \begin{bmatrix} X_4 & X_5 & \cdots & X_n \end{bmatrix} \end{aligned} \tag{15}$$

Model-IV

$$\begin{aligned} \boldsymbol{X}_{input}^{f} &= \begin{bmatrix} X_1 & X_2 & \cdots & X_{n-4} \\ X_2 & X_3 & \cdots & X_{n-3} \\ X_3 & X_4 & \cdots & X_{n-2} \\ X_4 & X_5 & \cdots & X_{n-1} \end{bmatrix} \\ \boldsymbol{X}_{output}^{f} &= \begin{bmatrix} X_5 & X_6 & \cdots & X_n \end{bmatrix} \end{aligned} \tag{16}$$

Assuming that the length of the training data is n, the structure monitoring data X_i are first normalized. The GRU neural network models are trained in accordance with the above four configurations of the network input and output. The GRU neural network model includes one GRU layer and one fully connected layer. In the training process, the grid search algorithm is used to optimize the hyperparameters of the network model.[22] The optimized learning rate and number of GRU units are 0.005 and 90, respectively. In addition, the Adam optimizer is used in network backpropagation during the training process.

After training, the GRU neural network models are used to predict the test data. The beam-end displacement and pylon tower tilt prediction results are shown in Figs. 5(a) and 6(a), respectively. Similarly, the LSTM neural network models with the same input and output configurations are also trained by using the same hyperparameter optimization algorithm. The test data are also predicted by the LSTM neural network models and the results are shown in Figs. 5(b) and 6(b), respectively.

It can be seen in Figs. 5 and 6 that the prediction results of the test data for both the GRU and LSTM neural network models have high waveform consistency with the monitoring data in the time domain. The errors between the test data and the prediction results are clearly observed in the figure. The numerical deviation of the prediction results of Model II is the smallest, while the deviation of Model IV is the largest. By comparison with the waveform deviation of the time

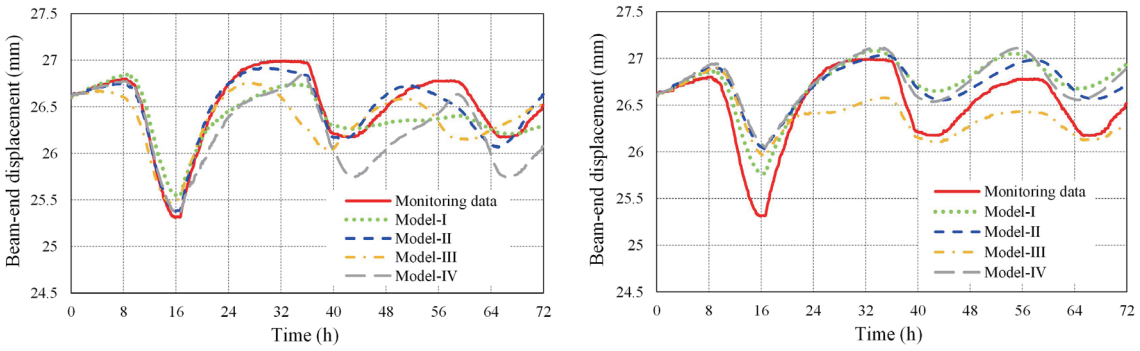

Fig. 5. (Color online) Prediction results of the test beam-end displacement data: (a) GRU and (b) LSTM.

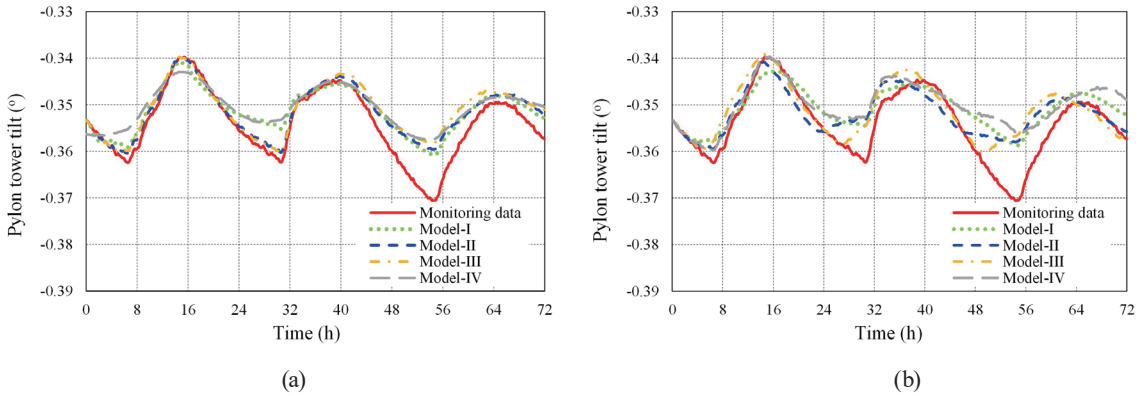

Fig. 6. (Color online) Prediction results of the test pylon tower tilt data: (a) GRU and (b) LSTM.

domain data sequences, the errors of the LSTM neural network models appear larger than those of the GRU neural network models. To evaluate the prediction accuracy of the four network models more quantitatively, the root mean square error (*RMSE*) is adopted:[23]

$$RMSE = \sqrt{\frac{1}{n}\sum_{i=1}^{n}\left(Y_q - \hat{Y}_q\right)^2}, \tag{17}$$

where n is the length of the test data sequence, Y_q (q = 1, …, n) are the monitoring data, and $\widehat{Y_q}$ are the data predicted by neural network models. The *RMSE* values of the prediction results in Figs. 5 and 6 are calculated and shown in Fig. 7.

As shown in Fig. 7, Model II results in the minimum *RMSE* of the GRU and LSTM neural networks in the prediction of two data sequences. Figure 7 also shows that the prediction accuracy of the GRU neural network model is significantly higher than that of the LSTM neural network model. Therefore, we hereafter use the GRU neural network model (Model-II) to recover abnormal monitoring data.

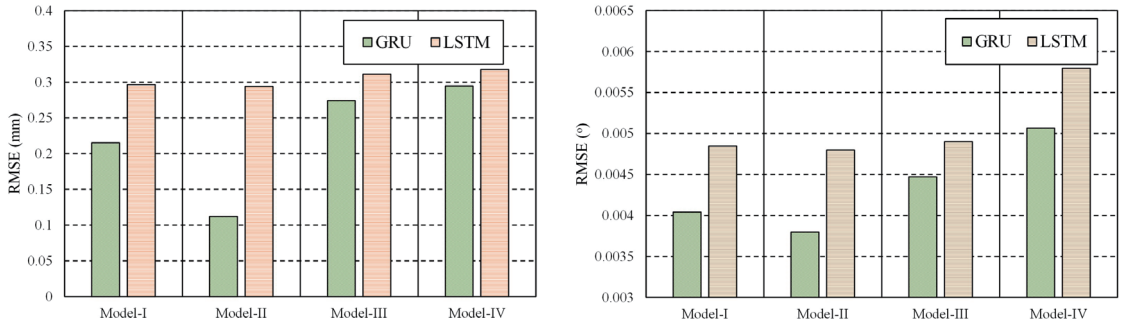

(a) (b)

Fig. 7. (Color online) *RMSE* of prediction results: (a) beam-end displacement and (b) pylon tower tilt.

3.3 Bidirectional prediction

Figures 5 and 6 further indicate that for the first 40 h, the errors between the predicted data and the monitoring data are relatively low. However, the prediction error increases and the accuracy decreases over the subsequent 32 h. When the prediction sequence is long, the accuracy of the GRU neural network model usually decreases. Most of the existing studies on data sequence prediction and recovery are based on forward prediction.[14–16] Forward prediction uses past information to predict future information, and it does not make full use of an information.

Considering the above understanding, in this study we propose an abnormal data recovery framework based on bidirectional prediction. This framework uses the data sequences before and after the abnormal data sequence to train the GRU neural network model. Then, the abnormal data sequence is recovered by bidirectional prediction. The bidirectional prediction for abnormal data recovery is as follows. First, the left training data sequence in Fig. 4 is used in forward training of the GRU neural network, of which the input and output configurations are Model II. Then, the test data sequence is recovered by forward prediction. Similarly, the right training data sequence in Fig. 4 is used in backward training of the GRU neural network with the same configuration (Model II). The test data sequence is recovered by backward prediction. The recovery results of forward and backward prediction of beam-end displacement data are shown in Fig. 8(a). The recovery results of forward and backward prediction of pylon tower tilt data are shown in Fig. 8(b). For the backward model, the predicted results from the 32nd hour to the 72nd hour are in good agreement with the actual monitoring data. However, the prediction accuracy of the data sequences before the 32nd hour is lower.

Therefore, to make full use of both the left and right sides of the abnormal data sequence, we propose a bidirectional prediction method for abnormal data recovery, which can make use of both the forward and backward prediction results. The bidirectional prediction results of the two data sequences are calculated using Eq. (12). The bidirectional prediction results are also shown in Fig. 8. The figure indicates that the bidirectional prediction results are almost completely consistent with the test data sequence. *RMSE* is also used to evaluate the accuracy of the three prediction results in the two data sequences in Fig. 8. The prediction errors are shown in Table 1.

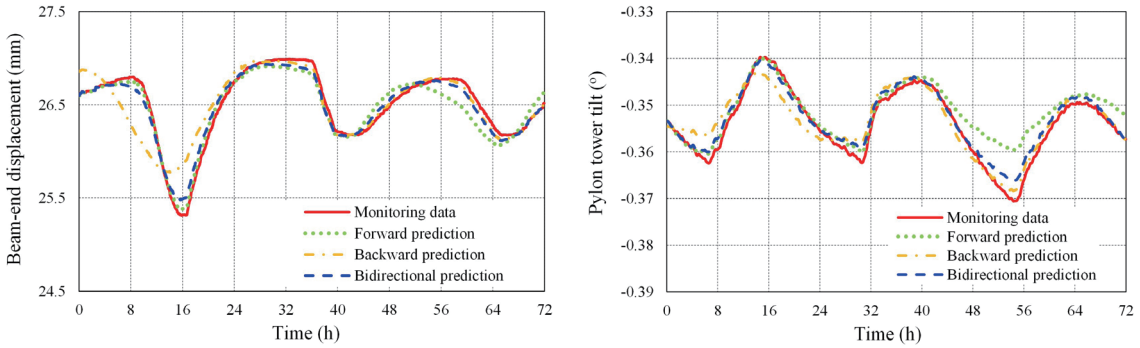

Fig. 8. (Color online) Prediction results: (a) beam-end displacement and (b) pylon tower tilt.

Compared with the unidirectional (forward or backward) prediction sequences, the *RMSE* of the bidirectional prediction sequence is significantly reduced. Therefore, the bidirectional prediction method can make full use of the information of the whole data sequence and effectively improve the accuracy of the GRU neural network for long-distance sequence prediction and abnormal data recovery.

4. Abnormal Data Recovery

The framework proposed above is used to recover abnormal monitoring data of Waitan Bridge. The monitoring data sequences of beam-end displacement sensor BDS_1-1 and cable tower tilt sensor PTS_1-1 from August 21 to August 27, 2020 are selected. As shown in Figs. 9(a) and 10(a), there are outliers and missing data in data segments A and B, respectively. After abnormal data are eliminated, the monitoring data are recovered by using the data recovery framework. A two-day data sequence, which contains 1440 data points before each abnormal data segment, is selected to train the GRU neural network model for forward prediction. Similarly, a two-day data sequence of data after each abnormal data segment is also selected to train the backward prediction model. Finally, bidirectional prediction is carried out to recover the eliminated abnormal data. The data recovery results are shown in Figs. 9(b) and 10(b). The regular diurnal variation of the normal monitoring data can be found in the recovered data. The results in the figure indicate that abnormal data recovery ensures the integrity and practicability of the monitoring data of the bridge.

To further demonstrate incorrect structural assessment caused by abnormal monitoring data, Figs. 11(a) and 12(a) show the correlation scatter plots of beam-end displacement–(structural) temperature and pylon tower tilt–temperature. In the figures, the linear regression equations of the structural responses and the structural temperature are also presented. In the equations, D, P, and T denote the beam-end displacement, pylon tower tilt, and structural temperature, respectively. The scatter points of abnormal data are also shown. It is found that the coefficients of determination R^2 of the two linear equations are low. Hence, abnormal data should be recovered to regain the accuracy and integrity of the monitoring data.

Figures 11(b) and 12(b) show the correlation scatter plots of beam-end displacement–temperature and pylon tower tilt–temperature after abnormal data recovery. Compared with the

Table 1
GRU neural network prediction error.

Prediction	Forward	Backward	Bidirectional
Beam-end displacement	0.1120	0.2073	0.0768
Pylon tower tilt	0.0037	0.0026	0.0017

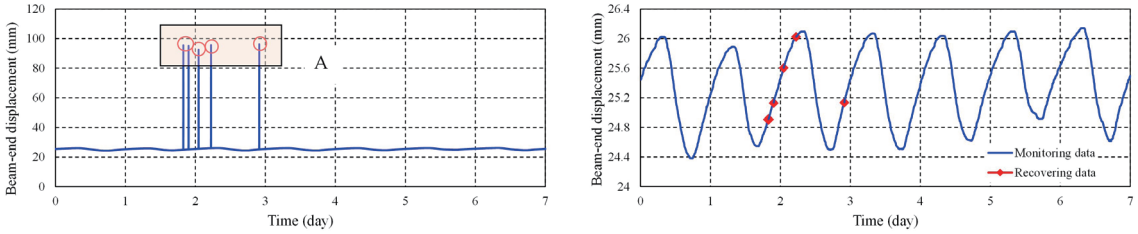

(a) (b)

Fig. 9. (Color online) Beam-end displacement data: (a) original monitoring data and (b) recovery results.

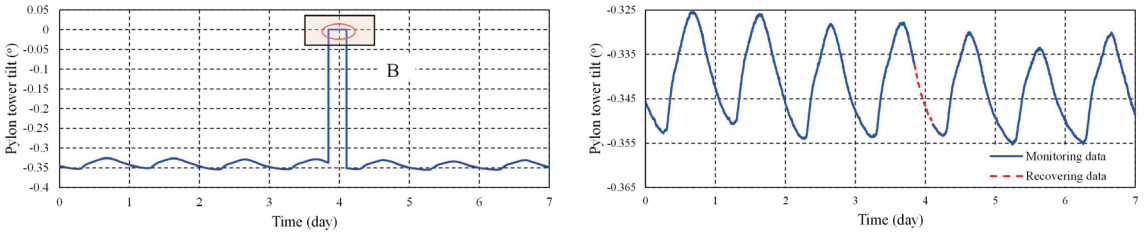

(a) (b)

Fig. 10. (Color online) Pylon tower tilt data: (a) original monitoring data and (b) recovery results.

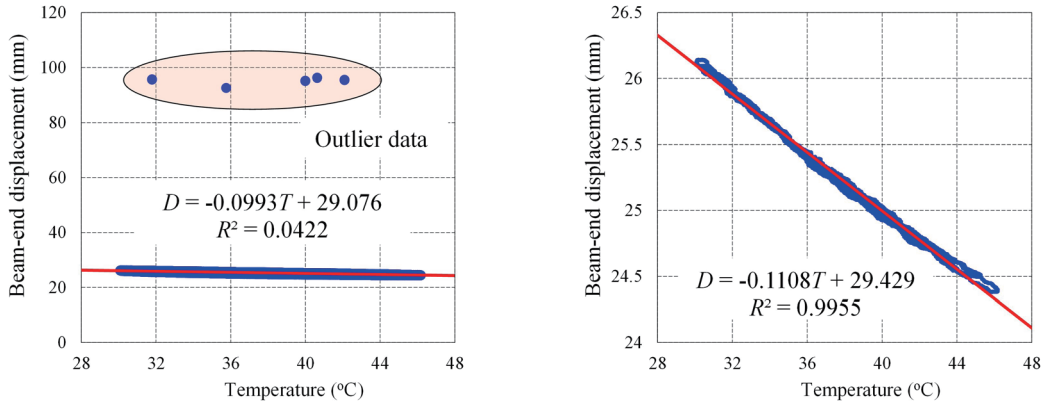

(a) (b)

Fig. 11. (Color online) Correlation scatter plots of beam-end displacement BDS_1-1 and structure temperature ST-1: (a) original monitoring data and (b) recovery results.

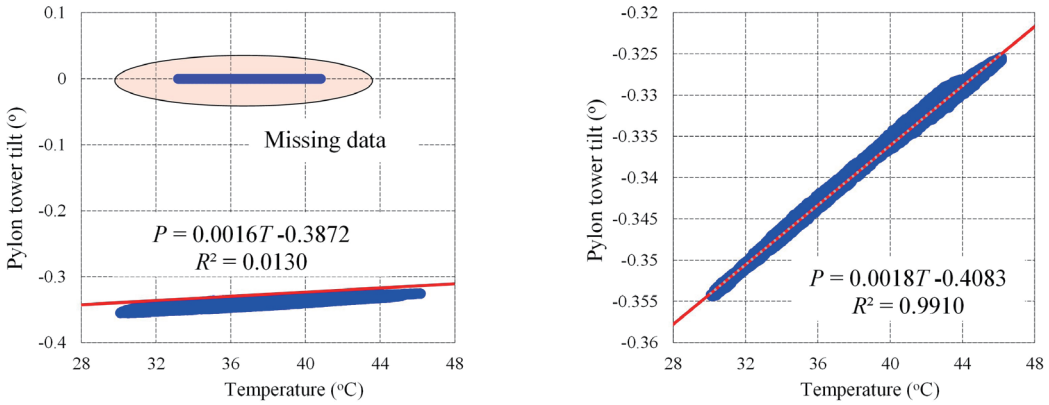

Fig. 12. (Color online) Correlation scatter plots of pylon tower tilt PTS_1-1 and structure temperature ST-2: (a) original monitoring data and (b) recovery results.

results in Figs. 11(a) and 12(a), the coefficients of determination R^2 are greatly improved to more than 0.9. This means that more accurate and reasonable linear regression equations of beam-end displacement–temperature and pylon tower tilt–temperature are obtained. This study demonstrates that abnormal monitoring data recovery can restore the actual structural response to a great extent and ensure the integrity and practicability of the monitoring data. The reliability of structural state assessment based on structural monitoring data for the bridge is thus improved.

5. Conclusions

(i) There is usually much abnormal monitoring data in structural health monitoring systems. Such abnormal monitoring data seriously affect the accuracy and efficiency of data analysis, making it difficult to obtain accurate structural states.

(ii) We propose a framework for abnormal data recovery based on a GRU neural network and temporal correlation. The framework is independent of variable correlation and adjacent sensors. To improve the prediction accuracy of the proposed framework, the configurations of the input and output of the network are optimally determined. To make full use of the monitoring data, bidirectional prediction is introduced in the abnormal data recovery framework.

(iii) The recovery results show that the accuracy of the GRU neural network is markedly higher than that of the LSTM network. Moreover, the linear correlation between structural response and temperature is greatly improved after abnormal data recovery. The structural abnormal monitoring data recovery framework proposed in this study can restore the actual structural response to a great extent and ensure the integrity and accuracy of the data. The proposed framework is suitable for the recovery of static or regular structural monitoring data.

Acknowledgments

This work was supported by the National Natural Science Foundation of China (51878027), the Beijing Municipal Education Commission (CIT&TCD201904060), and the Fundamental Research Funds for Beijing University of Civil Engineering and Architecture (X20174).

References

1 H. Zhang, Y. Liu, and Y. Deng: Adv. Struct. Eng. **24** (2020) 947. https://doi.org/10.1177/1369433220971779
2 C. Kim, K. Chang, P. McGetrick, S. Inoue, and S. Hasegawa: Sens. Mater. **29** (2017) 153. https://doi.org/10.18494/SAM.2017.1433
3 S. Feng and J. Jia: Struct. Health Monit. **17** (2018) 169. https://doi.org/10.1177/1475921716688372
4 Z. Nie, J. Lin, J. Li, H. Hao, and H. Ma: Struct. Health Monit. **19** (2019) 917. https://doi.org/10.1177/1475921719868930
5 Z. Tang, Z. Chen, Y. Bao, and H. Li: Struct. Control Health Monit. **26** (2019) e2296. https://doi.org/10.1002/stc.2296
6 T. Nagayama, S. Sim, Y. Miyamori, and B. Spencer: Smart Struct. Syst. **3** (2007) 299. https://doi.org/10.12989/sss.2007.3.3.299
7 G. Fan, J. Li, and H. Hao: Struct. Control Health Monit. **26** (2019) e2433. https://doi.org/10.1002/stc.2433
8 B. Eskelson, H. Temesgen, V. Lemay, T. Barrett, N. Crookston, and A. Hudak: Scand. J. For. Res. **24** (2009) 235. https://doi.org/10.1080/02827580902870490
9 I. Farreras-Alcover, M. Chryssanthopoulos, and J. Andersen: Struct. Health Monit. **14** (2015) 648. https://doi.org/10.1177/1475921715609801
10 H. Wan and Y. Ni: Struct. Health Monit. **18** (2018) 1282. https://doi.org/10.1177/1475921718794953
11 L. Li, H. Liu, H. Zhou, and C. Zhang: Adv. Eng. Software **149** (2020) 102901. https://doi.org/10.1016/j.advengsoft.2020.102901
12 Z. Zhang and Y. Luo: Mech. Syst. Sig. Process. **91** (2017) 266. https://doi.org/10.1016/j.ymssp.2017.01.018
13 Y. Ma, Y. He, L. Wang, and J. Zhang: Probab. Eng. Mech. **69** (2022) 103264. https://doi.org/10.1016/j.probengmech.2022.103264
14 G. Fan, J. Li, and H. Hao: Struct. Control Health Monit. **26** (2019) e2433. https://doi.org/10.1002/stc.2433
15 S. Jeong, M. Ferguson, R. Hou, J. Lynch, H. Sohn, and K. Law: Adv. Eng. Inf. **42** (2019) 100991. https://doi.org/10.1016/j.aei.2019.100991
16 R. Yuan, C. Su, E. Cao, S. Hu, and H. Zhang: Appl. Sci. **11** (2021) 7334. https://doi.org/10.3390/app11167334
17 H. Zhao, Y. Ding, A. Li, W. Sheng, and F. Geng: Struct. Control Health Monit. **27** (2020) e2618. https://doi.org/10.1002/stc.2618
18 J. Yang, F. Yang, Y. Zhou, D. Wang, R. Li, G. Wang, and W. Chen: Inf. Sci. **566** (2021) 103. https://doi.org/10.1016/j.ins.2021.02.064
19 D. Choe, H. Kim, and M. Kim: Renewable Energy **174** (2021) 218. https://doi.org/10.1016/j.renene.2021.04.025
20 H. Jiang, C. Wan, K. Yang, Y. Ding, and S. Xue: Struct. Health Monit. **21** (2021) 1093. https://doi.org/10.1177/14759217211021942
21 Z. Yue, Y. Ding, and H. Zhao: J. Bridge Eng. **26** (2021) 05021004. https://doi.org/10.1061/(ASCE)BE.1943-5592.0001716
22 S. Li, S. Li, S. Laima, and H. Li: Struct. Control Health Monit. **28** (2021) e2772. https://doi.org/10.1002/stc.2772
23 Y. Chang, H. Chiao, S. Abimannan, Y. Huang, Y. Tsai, and K. Lin: Atmos. Pollut. Res. **11** (2020) 1451. https://doi.org/10.1016/j.apr.2020.05.015

About the Authors

Hanwen Ju received his B.E. degree from Beijing University of Civil Engineering and Architecture, China, in 2020. Since 2020, he has been a graduate student at Beijing University of Civil Engineering and Architecture. His research interest is structural health monitoring. (jhwrrr@sina.com)

Yang Deng received his Ph.D. degree from Southeast University, China, in 2011. From 2011 to 2014, he was an assistant professor at Changsha University of Science and Technology, China. From 2015 to 2017, he was an associate professor at Changsha University of Science and Technology. Since 2020, he has been a professor at Beijing University of Civil Engineering and Architecture. His research interest is structural health monitoring. (dengyang@bucea.edu.cn)

Wenqiang Zhai received his B.E. degree from Southwest Jiaotong University, China, in 2019. Since 2020, he has been a graduate student at Beijing University of Civil Engineering and Architecture, China. His research interest is structural health monitoring. (952669880@qq.com)

Aiqun Li received his Ph.D. degree from Southeast University, China, in 1992. He has been a professor at Beijing University of Civil Engineering and Architecture since 2015. His research interests are disaster prevention, mitigation engineering, and structure health monitoring. (liaiqun@bucea.edu.cn)